Air Cathode Catalysts of Microbial Fuel Cell by Nitrogen-Doped Carbon Aerogels

Wei Yang[a,b,c], Yi Peng[c], Yudong Zhang[a,b], Jia En Lu[c], Jun Li[* a,b] and Shaowei Chen[*c]

[a] Key Laboratory of Low-grade Energy Utilization Technologies and Systems (Chongqing University), Ministry of Education, Chongqing 400030, China. E-mail: lijun@cqu.edu.cn

[b] Institute of Engineering Thermophysics, School of Energy and Power Engineering, Chongqing University, Chongqing 400030, China

[c] Department of Chemistry and Biochemistry, University of California, Santa Cruz, California 95060, USA. E-mail: shaowei@ucsc.edu
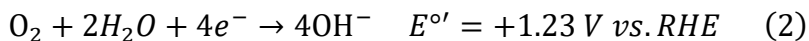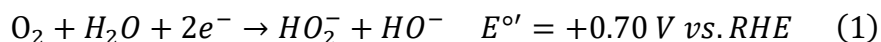
ABSTRACT

Microbial fuel cell (MFC) has been attracting extensive interest because it can be used for electricity generation and concurrently wastewater treatment. Yet, the MFC performance has remained limited due to the sluggish electron-transfer kinetics and hence high overpotential of oxygen reduction reaction (ORR) at the cathode. In the present study, nitrogen-doped carbon aerogels (NCAs) were prepared by pyrolysis of polyacrylonitrile at controlled temperatures (600

to 900 °C). Electrochemical tests showed apparent electrocatalytic activity by the NCAs towards ORR in alkaline media, and among the series the sample prepared at 800 °C exhibited the best performance, with a half-wave potential of +0.80 V vs. RHE and the number of electron transfer around 3.9. The electrocatalytic performance was ascribed to nitrogen doping that generated catalytic active sites and led to improved ORR kinetics. An MFC using the best NCA as cathode catalysts achieved a maximum power density of 1048 ± 47 mW m^{-2}, close to that (1051 ± 28 mW m^{-2}) based on state-of-art Pt/C, and a mass specific power of 52.4 mW g^{-1}. These results demonstrate that cost-efficient NCAs can be used as a viable, platinum-free, ORR catalyst for MFC applications.

Introduction

Because of energy crisis and environmental pollution arising from the combustion of fossil fuels, development of effective technologies for renewable energy conversion and storage has been attracting extensive interest.[1-4] Among these, microbial fuel cell (MFC) has been hailed as a unique energy device that can not only produce electricity but also concurrently treat wastewater.[5] In an MFC, select microorganisms are loaded onto the anode, where organic matters in wastewater are oxidized generating electrons and protons. These are then transferred to the cathode where reduction of oxygen to water occurs.[6] The design of MFC can be simplified with an air cathode by taking advantage of the ready accessibility of oxygen from air. This has indeed been exploited as a promising configuration for practical applications. Note that the MFC performance can be impacted by several factors, including anode/cathode structure, exoelectrogenic bacteria on anode, anode biofilm, growth media, and oxygen reduction reaction (ORR) kinetics at cathode. Among these, the sluggish kinetics and high overpotential of ORR has been recognized as a major bottleneck that limits the MFC performance.[7]

Prior studies have shown that ORR at the air cathode of MFCs generally proceeds via two pathways,[8-9]

$$O_2 + H_2O + 2e^- \rightarrow HO_2^- + HO^- \quad E^{\circ\prime} = +0.70\ V\ vs.\ RHE \quad (1)$$

$$O_2 + 2H_2O + 4e^- \rightarrow 4OH^- \quad E^{\circ\prime} = +1.23\ V\ vs.\ RHE \quad (2)$$

One is the 2e⁻ pathway with peroxide species as the product (reaction 1), and the other is the 4e⁻ pathway where oxygen is fully reduced to hydroxide (reaction 2). Apparently, the four-electron pathway produces a higher ORR potential at the cathode, leading to a higher power density in MFC, and hence is preferred over the two-electron route. In fact, extensive research has been carried out in catalyst design and engineering to reduce ORR overpotential and to facilitate the four-electron pathway.[11-12] Typical ORR catalysts in MFC entail three groups: noble metals,[13-14] non-noble metals,[15-16] and carbon-based catalysts.[17-18] Platinum and its alloy have been used as the leading catalysts towards ORR, but the applications have been severely hampered due to their high costs and unsatisfactory durability, as they are prone to inactivation due to poisoning and biofouling under relevant MFC conditions.[19-20]

Notably, carbon-based catalysts have emerged as viable MFC air cathode catalysts, due to their considerable catalytic activity, high chemical and mechanical stability, poison tolerance, and low costs.[21-22] Heteroatoms doping in carbon-based catalysts is an effective approach to form abundant active sites.[23] Of these, carbons doped with nitrogen or codoped with metal and nitrogen are two kinds of commonly used catalysts. For instance, Yang et al.[27] observed that Fe,N-codoped carbon was a viable catalyst for ORR with a half-wave potential ($E_{\frac{1}{2}}$) of +0.813 V vs. RHE in 0.1 M H_2SO_4. Nitrogen-doped carbon nanotubes have also been used as low-cost and durable ORR catalysts for MFC, and in comparison to Pt/C, the maximum power density (1600 ± 50 mW m⁻²) is about 15% higher.[12] In another study,[25] an MFC was constructed using

nitrogen-doped graphene as the air cathode catalyst, where the maximum power density (1470 ± 80 mW m^{-2}) was found to be 32% higher than that with Pt/C. Doped carbons have also been prepared with carbon aerogels that feature a porous and amorphous carbon network structure.[28] For example, Tardy et al.[29] synthesized a nitrogen-doped carbon aerogel (NCA), used it as air cathode catalysts for MFC, and observed an outstanding performance, with a maximum power density of $37 \pm 0.8\,\mathrm{W\,m}^{-3}$. Similarly, Salvador et al.[30] prepared nitrogen-doped carbon-based aerogels as ORR catalysts for MFC, and obtained a mass specific power of 2.56 mW g^{-1}. These studies highlight the feasibility of NCA as effective ORR catalysts for MFC. Notably, in these studies NCAs are usually prepared by using separate carbon and nitrogen precursors, and post-synthesis engineering is needed to increase nitrogen dopant concentration in the samples. This not only requires massive use of nitrogen-containing chemicals but also complicates the preparation procedure.

In the present study, we describe pyrolytic preparation of nitrogen-doped carbon aerogels (NCAs) as MFC air cathode catalysts from a single precursor, nitrogen-enriched polyacrylonitrile, at elevated temperatures (600 to 900 °C). The obtained NCAs showed high nitrogen contents at 8 to 24 at.% and exhibited remarkable ORR activity in alkaline media, and an MFC based on the NCA cathode was constructed to evaluate the feasibility in practical applications. The power density was found to be competitive to that with a Pt/C cathode.

Experiment section
Chemicals

Commercial Pt/C (20 wt.%, Alfa Aesar), acrylonitrile (Acros), ammonium persulfate (+99%, ACROS), Pluronic F127 (F127, Acros), and polytetrafluoroethylene (PTFE, 60 wt.% solution, Sigma Aldrich) were used as received. Nafion® was diluted to 20 wt.% before use. All solvents

were obtained at their highest purity from Fisher Scientific and also used as received. Water was purified by a Barnstead Nanopure water system (resistivity 18.3 MΩ cm).

Synthesis of NCA

Polyacrylonitrile was first prepared via an emulsion polymerization method based on a reported procedure with some modifications.[32] In brief, 30 mL of acrylonitrile was added into 250 mL of Nanopure water in a flask under magnetic stirring at room temperature. The solution was then deaerated with ultrahigh-purity N_2 for 30 min (flow rate 200 mL min^{-1}) and heated up to 60 °C in an oil bath, into which was injected 30 mg of ammonium persulfate dissolved in 30 mL of water, and after 30 min of reaction, a 15 mL water solution containing 1g of triblock copolymer Pluronic F127. The polymerization was continued for 6 h under N_2 bubbling to produce an emulsion solution of polyacrylonitrile, which was then subject to hydrothermal reaction at 180 °C for 6 h after being transferred into a 100 mL Teflon-lined autoclave. Then the autoclave was taken out of the oven, and the solution was cooled down naturally to ambient temperature. Polyacrylonitrile was obtained by filtration and subject to controlled pyrolysis in a tube furnace under a constant flow of nitrogen (flow rate 200 mL min^{-1}) at varied temperatures (i.e., 600, 700, 800 and 900 °C) for 2 h. The heating rate was set at 5 °C min^{-1}. When cooled down naturally to room temperature, the products (4 ~ 5 g) were collected and denoted as NCA600, NCA700, NCA800 and NCA900, respectively.

Structural Characterizations

Transmission electron microscopy (TEM) measurements were carried out with a Philips CM300 microscope operated at 300 kV. Dilute dispersions of the samples were prepared in ethanol and dropcast onto a TEM grid, which was dried at 40 °C in a vacuum oven. X-ray diffraction (XRD) studies were performed with a Rigaku Americas Miniflex Plus powder

diffractometer operated at 40 kV and 30 mA within the range of 5° to 90° at the scan rate of 1° min^{-1}. Raman spectra were collected on a LabRAM HR Evolution instrument using an Ar ion laser (514.5 nm). XPS measurements were conducted with a PHI 5400/XPS instrument operated with a 350 W Al Kα source at 10^{-9} torr.

Electrochemistry

Voltammetric studies were carried out on a CHI710 electrochemical workstation. Electrochemical impedance spectra were acquired with a Gamry Reference 600 instrument. A Ag/AgCl electrode (in 1 M KCl) was used as the reference electrode (which was calibrated against a reversible hydrogen electrode (RHE) at +0.222 V vs. RHE), a graphite rod (5 mm in diameter) as the counter electrode, and a rotating (gold) ring–(glassy carbon) disk electrode (RRDE) as the working electrode (the surface areas of the disk and ring electrodes were 0.246 and 0.188 cm^2, respectively). All potentials in the present study were referenced to the RHE. In the preparation of catalyst inks, 5 mg of the as-prepared NCA catalysts was dispersed in 2 mL of a mixture of water/ethanol (v:v = 1:2), into which was then added 20 μL of a Nafion solution. After sonication for 30 min to disperse the catalysts, 20 μL of the ink was cast onto the surface of the glassy carbon disk electrode in a dropwise fashion and dried at ambient temperature (prior to use, the RRDE was polished with 50 nm Al$_2$O$_3$ powders and extensively rinsed with Nanopure water), corresponding to a catalyst loading of 0.203 mg cm^{-2}.

In voltammetric tests, baseline currents were first obtained in N$_2$-saturated 0.1 M NaOH, and the electrocatalytic activity was then evaluated with the solution saturated with oxygen. Prior to tests, the electrode was activated electrochemically by potential cycling within the range of +1.0 V to +0.2 V at the scan rate of 100 mV s^{-1} until steady voltammetric profiles were reached, so as to eliminate excess oxygen and/or contaminant species trapped within the carbon cavities. Linear

sweep voltammetric (LSV) tests were performed by sweeping the potential of the working electrode at the scan rate of 10 mV s^{-1} from +1 to 0 V at different rotation rates (400 to 2500 rpm). The ORR current was obtained by subtracting the current under nitrogen sparging from that under oxygen sparging. The number of electron transfer (n) and yield of hydrogen peroxide (H$_2$O$_2$%) during the ORR process at the disk electrode were calculated by RRDE collection experiments using the following equations,

$$n = \frac{4j_{disk}}{j_{disk}+j_{ring}/N} \tag{3}$$

$$H_2O_2\% = \frac{200j_{ring}}{j_{ring}+Nj_{disk}} \tag{5}$$

where j$_{disk}$ and j$_{ring}$ are the disk and ring current densities, respectively, and N is the ring collection efficiency (0.4) .

In the Tafel plots, j_K was estimated from the LSV curves based on the following equation,

$$j_K = \frac{j \bullet j_D}{(j_D - j)} \tag{5}$$

where j is the total current density, j$_K$ is the kinetic current density, and j$_D$ is the diffusion-limited current density.

The double layer capacitance of the catalysts was quantified by cyclic voltammetric (CV) measurements in the non-faradic region. Experimentally, CV cures were acquired within the potential range of +0.1 to +0.2 V at varied scan rates (from 20 to 100 mV s^{-1}). The double layer capacitance (C$_{dl}$) was estimated based on the slope of linear regression of the current density versus scan rate. The catalyst stability was evaluated by chronoamperometric measurements in oxygen-saturated 0.1 M NaOH at the potential of +0.7 V and at the rotation rate of 1600 rpm.

Assembly and set up of MFCs

To prepare air cathodes, a layer of the catalysts was coated onto a piece of teflonized carbon cloth (WOS 1002 PHYCHEMi Co. Ltd., China) at the NCA loading of 2 mg cm^{-2} and commercial Pt/C loading of 0.5 mg cm^{-2}, as previously described.[13] In brief, the carbon cloth was teflonized by brushing the PTFE solution onto one side and thermally treated at 370 °C for 20 min. This coating procedure was replicated four times to produce teflonized carbon. After that, the catalyst ink prepared above was cast onto the other side of the teflonized carbon cloth in a dropwise fashion and dried at 80 °C for 1 h.[33] Carbon cloth of 3 cm in diameter (projected area ~7 cm^2) was used directly as the anode after washing in acetone and cleaning in water. The thus-prepared air cathode and anode were then mounted onto the two opposite faces of a cubic MFC reactor of 28 mL in volume. The electrode spacing was 4 cm, and the reference-cathode spacing was 1 cm. The MFC was inoculated with anaerobic digester sludge containing exoelectrogenic bacteria. During the inoculation process, an external resistor of 1000 Ω was connected to the MFC. The growth medium was composed of Na_2HPO_4 (11.82 g L^{-1}), KH_2PO_4 (2.32 g L^{-1}), sodium acetate (2.04 g L^{-1}), NaCl (0.5 g L^{-1}), NH_4Cl (0.1 g L^{-1}), $MgSO_4 \cdot 7H_2O$ (0.1 g L^{-1}), $CaCl_2 \cdot 2H_2O$ (15 mg L^{-1}), and trace elements (1.0 mM).[21] The MFCs were tested under the fed-batch mode at room temperature (30 ± 1 °C). Analyte was replenished with a fresh medium (pH 7.2, and electrical conductivity 3.81 S m^{-1}) when the cell voltage diminished under 50 mV.

Polarization curves of the MFCs were obtained by potential sweeping at the scan rate of 0.2 mV s^{-1} from the open-circuit voltage (OCV) to 0.05 V. The cathode was the working electrode, and the anode was connected to the reference electrode and counter electrode. The power output of MFCs was calculated by P = VI, where V was the cell voltage and I was the cell current. The power density of MFCs was determined by normalizing the power to the projected area of the air cathodes (7 cm^2). The tests were repeated twice to ensure reproducibility of the data.

Electrochemical impedance spectra were recorded at OCP with a 10 mV AC perturbation amplitude and the AC frequency varied from 100 kHz to 10 mHz. The tests were carried out in the same MFC reactor, where the air-cathode of the as-prepared NCA samples served as the working electrode, the Ag/AgCl (saturated KCl) electrode as the reference electrode, and the anode as the counter electrode. The Nyquist plots were fitted by EClab 11.10 according to an equivalent circuit.[34]

Results and discussion

The structure of the obtained NCA samples was firstly characterized by TEM measurements. From the representative TEM images of NCA800 in Fig. 1, one can see that the sample consisted of a number of particle-like structures, which aggregated into a carbon aerogel (Fig. 1a, b). At high magnification (Fig. 1c), the aerogel can be seen to entail hollow carbon structures, with a shell thickness of about 2.7 nm, which might result from the decomposition of Pluronic F127 templates at elevated temperatures.[35] The formation of such a carbon network led to a large contact interface between the electrolyte and the carbon catalyst, and the thin carbon shells reduced the diffusion distance from the electrolyte media to the interior of the carbon matrix, both of which facilitated mass transfer in the carbon catalyst layer.[36-37] Furthermore, in high-resolution TEM measurements (Fig. 1d), the samples can be seen to exhibit clearly-defined lattice fringes, with interplanar distances of 0.390 nm and 0.408 nm that were in good agreement with the graphitic carbon (120) and (222) planes,[38] respectively.
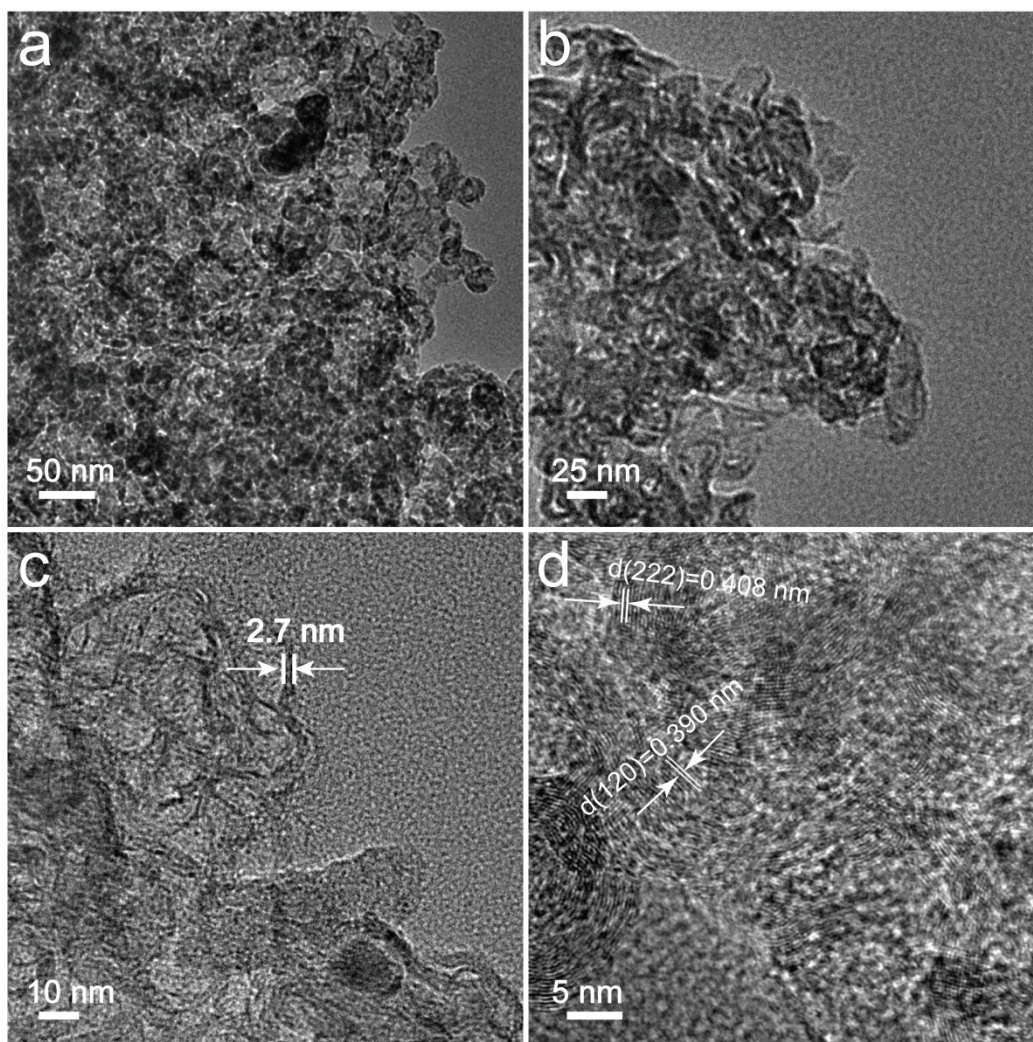
Fig. 1 Representative TEM images of NCA800 at varied magnifications.

The XRD patterns of the NCA samples prepared at different temperatures are shown in Fig. 2. Two main peaks can be identified for all samples at around 25° and 45°, corresponding to the diffractions of the (002) and (101) faces of the graphitic framework, respectively.[38] The broad peaks suggest limited graphitization and reduced crystallinity of the carbon aerogels. In addition, one can see that the (002) diffraction shifted slightly from 23.63° for NCA600 to 24.39° for NCA800 and NCA900, implying a shrinking interlayer spacing with increasing pyrolysis temperature, which was probably due to an increasing loss of nitrogen dopants at elevated temperatures. Concurrently, one can see that the peak at 45° became intensified, indicating

enhanced graphitization of the NCA samples. The structural defects and degree of graphitization of NCA was further examined by Raman spectroscopic measurements. From Fig. 2b, it can be seen that the NCA samples all displayed a D band at 1352 cm^{-1} and a G band at 1580 cm^{-1}.[39] In addition, the ratio of the D-band to G-band intensity (I_D/I_G) can be seen to decrease from NCA600 to NCA900 at 2.31, 2.21, 1.56 and 1.37 (Table 1), respectively. This, again, suggests that increasing pyrolysis temperature enhanced graphitization of the NCA samples, consistent with the XRD results.
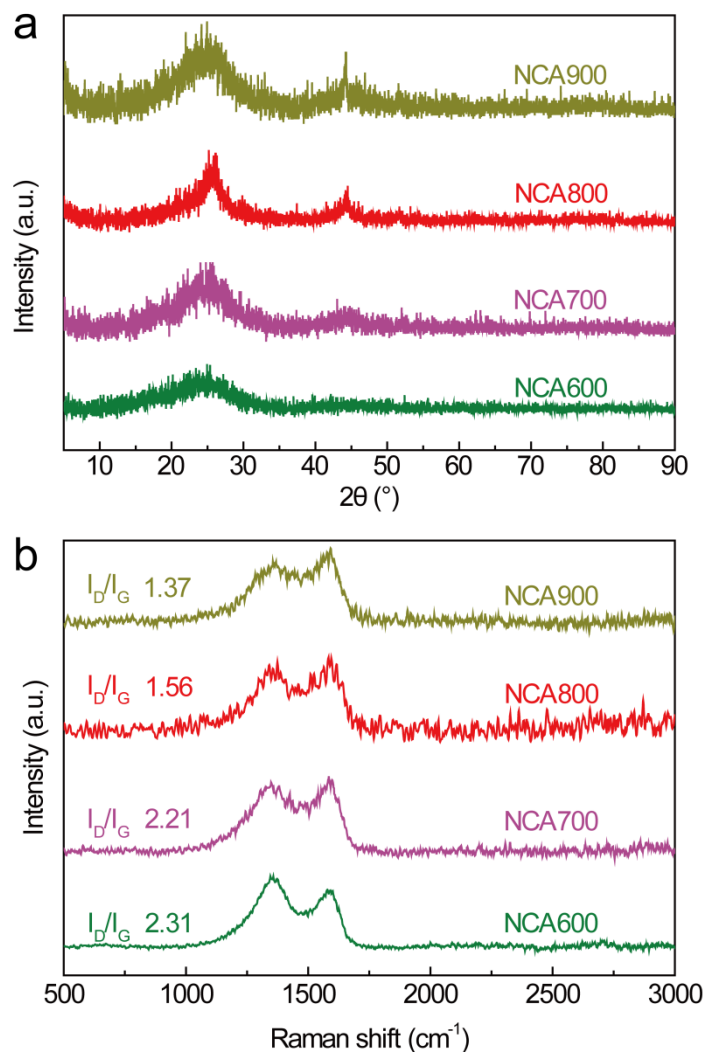

Fig. 2 (a) XRD patterns and (b) Raman spectra of NCA600, NCA700, NCA800 and NCA900.
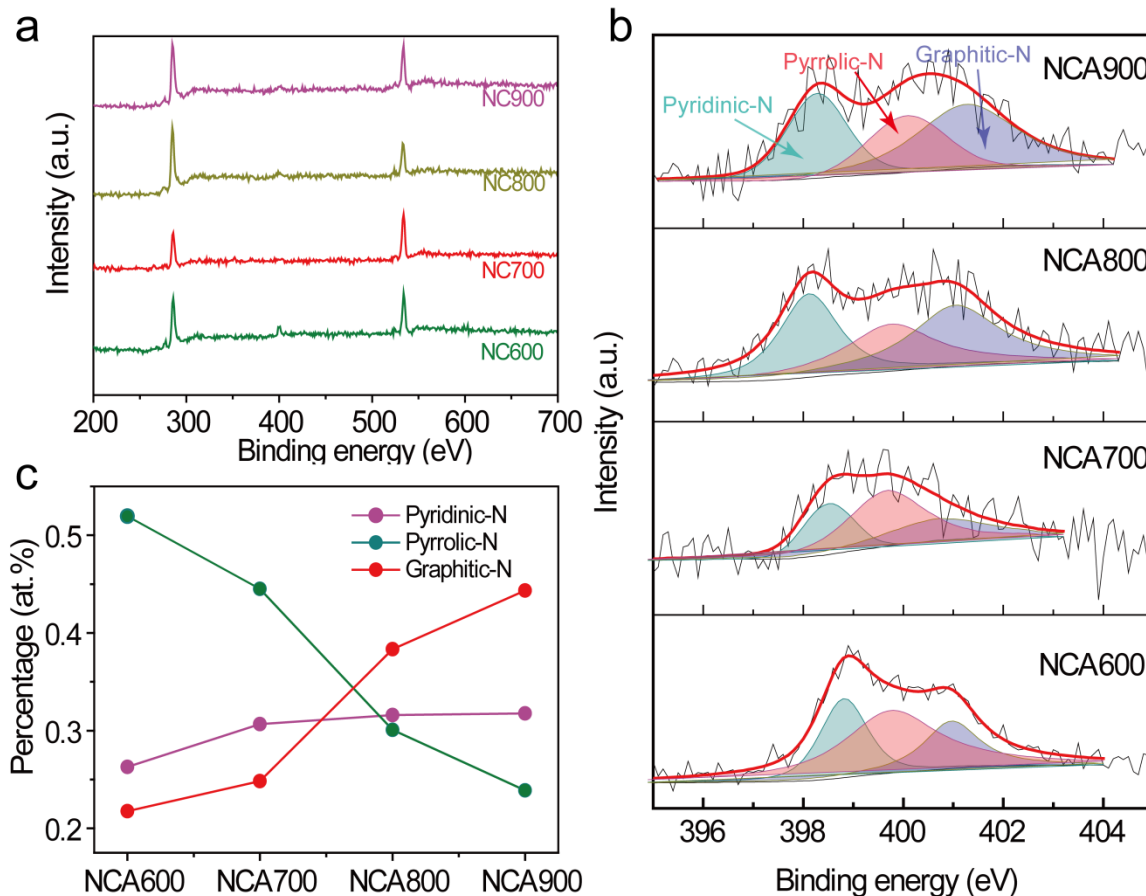
Fig. 3 (a) XPS full spectra of the series of NCA samples, and (b) high-resolution scans of the N 1s electrons. Black cures are experimental data and colored shades are deconvolution fits. (c) The relative contents of pyridinic-N, pyrrolic-N and graphitic-N in the NCA samples.

The elemental composition of the NCA catalysts was then evaluated by XPS analysis. From the XPS survey profiles in Fig. 3a, the C 1s, N 1s, O 1s electrons can be clearly found at about 284, 400, and 533 eV, respectively. This confirmed that nitrogen was indeed doped into the carbon matrix, at the concentration of 23.39 at.% for NCA600, 8.51 at.% for NCA700, 13.56 at.% for NCA800 and 10.4 at.% for NCA900 (Table 1), on the basis of the integrated peak areas. To identify the exact chemical configuration of the nitrogen dopants, high-resolution N 1s spectra were recorded for all samples. As shown in Fig. 3b, deconvolution of the N 1s spectra yielded three subpeaks, pyridinic-N at 398.4 eV, graphitic-N at 401.0 eV, and pyrrolic-N at

399.9 eV.[40-44] From Fig. 3c and Table 1, one can see that NCA800 exhibited the highest concentration (5.2 at.%) of graphitic-N among the samples, whereas the contents of pyridinic-N and pyrrolic-N were the highest with NCA600.

The ORR activity of the as-prepared NCAs was then evaluated and compared by voltammetric measurements. From Fig. 4a and Fig. S1, all samples can be seen to exhibit nonzero currents as the electrode potential swept cathodically in oxygen-saturated 0.1 M NaOH, suggesting apparent ORR activity, and increasing rotation rate led to an increase of the current, which became almost invariant at potentials below +0.6 V. The electrochemical performance of the various catalysts was then compared at the rotation rate of 1600 rpm, where $E_{\frac{1}{2}}$ can be estimated to be +0.72 V for NCA600, +0.75 V for NCA700, +0.80 V for NCA800 and +0.79 V for NCA900, along with a respective onset potential (E_{onset}) of +0.81, +0.82, +0.85 and +0.84 V (Fig. 4b and Table 1). From these results, NCA800 can be seen to exhibit the best activity among the series, which most probably arose from the combined results of a relatively high pyridinic-N and graphitic-N contents and high degree of graphitization (Table 1). Previously, it has been shown that the relative content of pyridinic-N and/or graphitic-N largely dictated the ORR activity of nitrogen-doped carbons. For instance, Lai et al.[45] showed that the onset potentials could be improved by pyridinic-N, and the limiting current density increased by graphitic-N. A consistent conclusion was reached by Wang et al.[44] where the attenuation of the ORR activity of nitrogen-doped carbons was correlated with the nitrogen dopant concentration, from which graphitic N was identified as the active sites for ORR. Notably, whereas NCA600 exhibited the highest content of pyridinic-N and only a slightly lower graphitic-N content than NCA800, the ORR performance was markedly lower. This was likely due to the much more defective carbon structures, as manifested in Raman measurements (Table 1), that compromised the effective electrical

conductivity and accessibility of the electrocatalytic active centers. That is, the ORR performance is a holistic reflection of the overall materials structures.
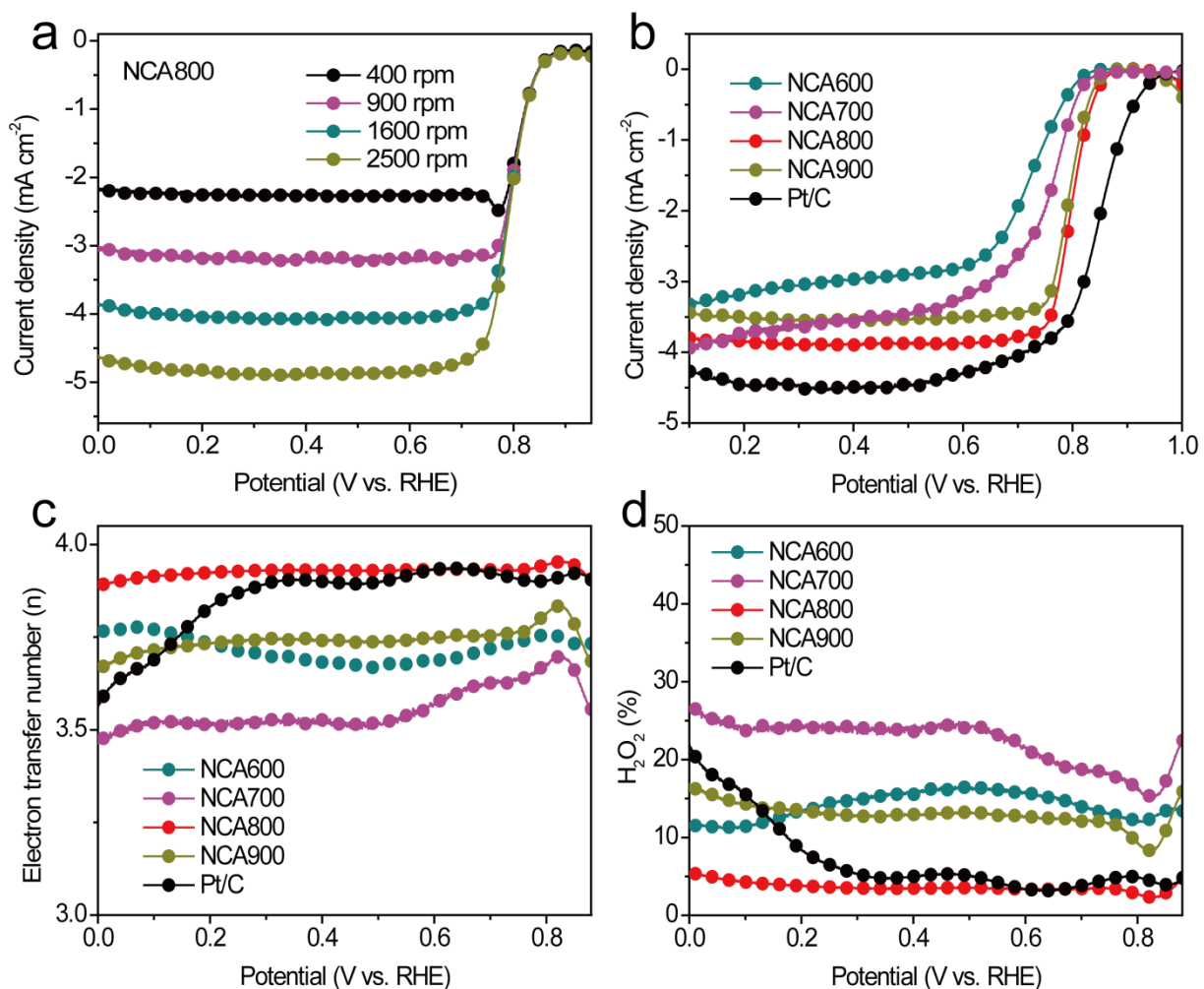

Fig. 4 (a) LSV curves of NC800 at different rotation rates in oxygen-saturated 0.1 M NaOH. (b) LSV curves in oxygen-saturated 0.1 M NaOH at the rotation rate of 1600 rpm, (c) number of electron transfer (n), and (d) H_2O_2 yield of NCA600, NCA700, NCA800, NCA900, and Pt/C.

To further evaluate the ORR performance, the number of electron transfer (n) was estimated by eq. 3 using the disk and ring currents at 1600 rpm. The n values of all catalysts were higher than 3.5 (Fig. 4c). For instance, n = 3.9 for Pt/C at +0.6 V, and it was the same for NCA800 (3.9), but lower for NCA600 (3.7), NCA700 (3.6) and NCA900 (3.7). These results indicate that

ORR on the NCA samples and Pt/C mostly proceeded via the 4e$^-$ pathway. The corresponding H$_2$O$_2$ yield was quantitatively evaluated by eq. (4). As depicted in Fig. 4d, the NCA samples can all be seen to exhibit a H$_2$O$_2$ yield less than 30% in the wide potential range of 0 to +0.9 V. Of these, the H$_2$O$_2$ yield of the NCA800 sample was only 3.4% at +0.6 V, again, similar to that of Pt/C (3.4%) but markedly lower than those of NCA600 (15.7%), NCA700 (21.6%) and NCA900 (12.7%).
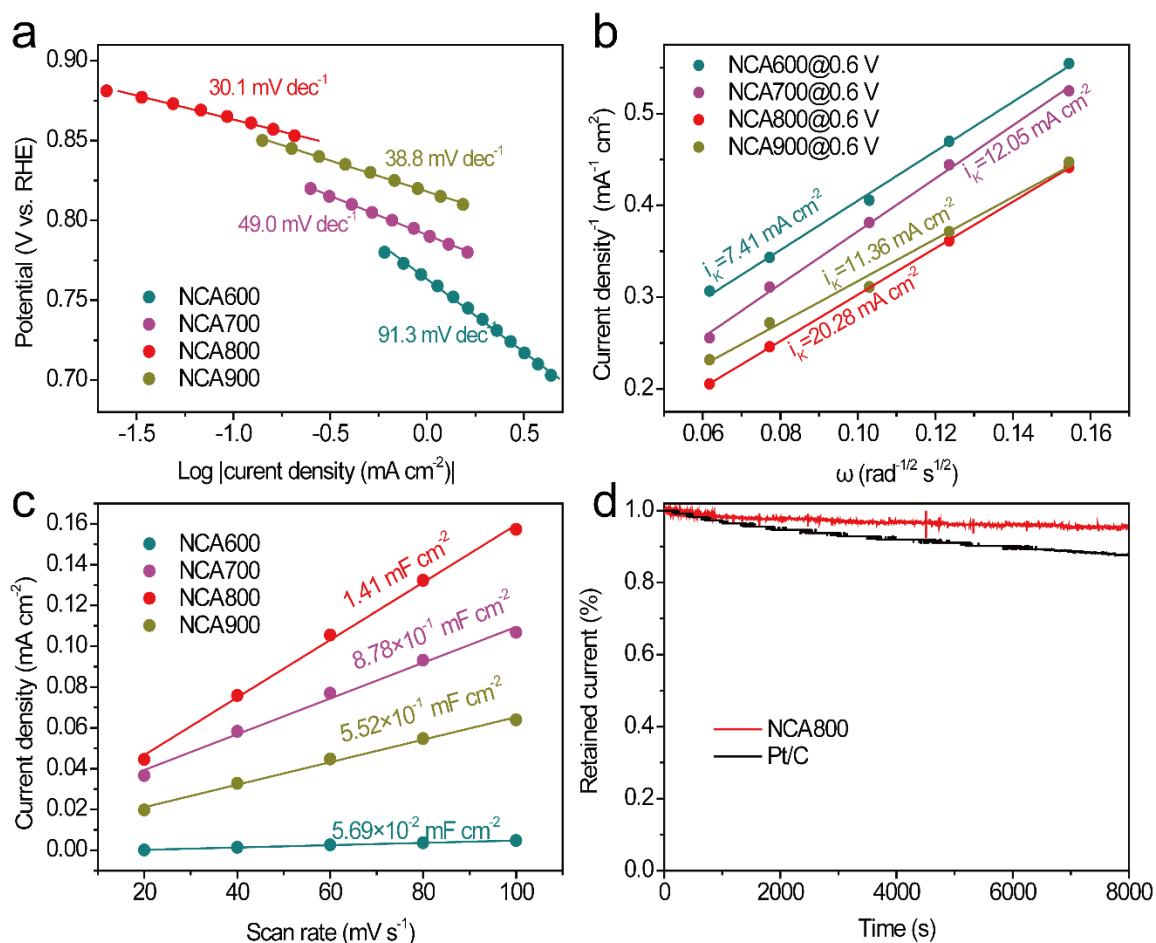

Fig. 5 (a) Tafel plots derived from LSV curves, (b) Koutecky-Levich plots at +0.6 V, (c) plots of the double-layer charging currents at +0.15 V versus scan rate, and (d) retention of ORR current at NCA800 and Pt/C over time at +0.7 V.

Further analysis was carried out with the Tafel plots (Fig. 5a) and Koutecky-Levich plots (Fig. 5b). It can be seen that NCA800 displayed the highest kinetic current density (j_K) and lowest Tafel slope among the series: 7.41 mA cm^{-2} and 91.3 mV dec^{-1} for NCA600, 12.05 mA cm^{-2} and 49.0 mV dec^{-1} for NCA700, 20.25 mA cm^{-2} and 30.1 mV dec^{-1} for NCA800, and 11.36 mA cm^{-2} and 38.8 mV dec^{-1} for NCA900. Again, this can be ascribed to the combined contributions of a relatively high graphitic-N concentration and good degree of graphitization of the carbon matrix. This can be further confirmed by the effective electrochemical surface area (ECSA), which is directly related to the electrode double-layer capacitance (C_{dl}). Fig. S2 shows the cyclic voltammograms of the NCA catalysts at various potential scan rates (20 to 100 mV s^{-1}) within the nonfaradaic potential range of +0.1 to +0.2 V, and C_{dl} was estimated by linear regression of the voltammetric current vs the potential scan rate (Fig. 5c), which was 5.69×10^{-5} mF cm^{-2} for NCA600, 5.54×10^{-4} mF cm^{-2} for NCA700, 1.41×10^{-3} mF cm^{-2} for NCA800, and 8.78×10^{-4} mF cm^{-2} for NCA900. Again, the C_{dl} was the highest with NCA800. That is, the high surface accessibility of NCA800 likely facilitated the ORR electrocatalysis.

Catalyst stability is another important factor in practical applications, which can be evaluated by chronoamperometric measurements. From Fig. 5d, one can see that while the ORR current (at +0.7 V) for both NCA800 and Pt/C diminished slowly over time, NCA800 retained 95% of the initial current after 2 h's operation, markedly higher than Pt/C (88%), suggesting remarkable stability of the NCA800 sample. This is likely due to the enhanced resistance against poisoning species and relatively low spin density of the carbon active sites, as compared to conventional Pt catalysts.[43]

The feasibility of the NCA catalysts for fuel cell air cathode was then examined in a MFC reactor. Fig. 6a depicts the polarization and power density profiles of the MFC using NCA800 or

Pt/C as air cathode catalysts. The cell voltages of both MFCs can be seen to decrease with increasing current density; however, within the large range of current density from 0 to 7000 mA m^{-2}, the cell voltage was almost the same for NCA800 and Pt/C. In addition, the NCA800 MFC exhibited a maximum power density of 1048 $\pm$ 47 mW m^{-2}, which is comparable to that of the Pt/C MFC (1051 $\pm$ 28 mW m^{-2}). From the polarization curves of the anode and cathode, the NCA800 and Pt/C cathodes can also be seen to show a similar performance at different current densities (Fig. S3). The internal resistance of the cathodes was then evaluated by electrochemical impedance measurements, as shown in Fig. 6b. The data were fitted by using a program (EClab 11.10) according to the equivalent circuit depicted in Fig. 6b inset,[34] and the results were listed in Table S1. It can be found that although Pt/C cathode have a slightly lower ohmic and charge transfer resistance than NCA800, the total cathode resistance (including ohmic, charge transfer, interface and mass transfer resistance) is comparable (42.14 Ω for NCA800 and 46.40 Ω for Pt/C).
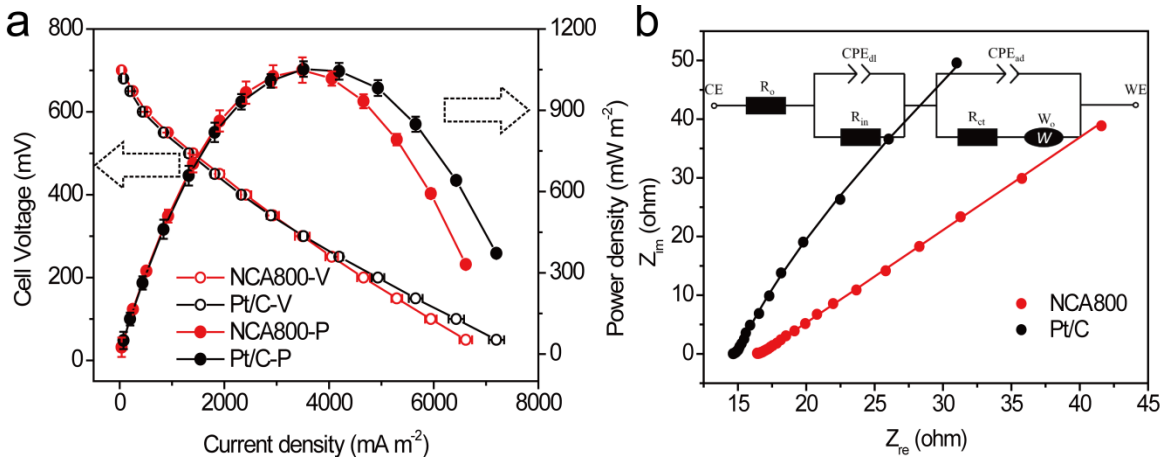

Fig. 6 (a) Polarization and power density profiles of an MFC with an NCA800 or Pt/C air cathode, and (b) the corresponding Nyquist plots at open circuit potential. Inset is the equivalent circuit, where R_t represents the total internal resistance, R_o the solution ohmic resistance, R_{in} the

interfacial ohmic resistance, R_{ct} the charge transfer resistance, C_{dl} the double layer capacitance, C_{ad} the pore adsorption capacitance, and W the Warburg impedance.

Significantly, one can see that the MFC performance with an NCA800 air cathode at a loading of 2 mg cm^{-2} was very competitive to that with Pt/C at the loading of 0.5 mg cm^{-2}. Yet, as compared to Pt, the low costs, remarkable ORR activity, and high electrocatalytic stability of NCA render it an attractive candidate as MFC cathode catalysts. To obtain a reasonable comparison with literature results, we normalized the power density by catalyst loading to obtain the mass specific power (MSP). It can be found that NCA800 displayed a high MSP of 52.4 mW g^{-1}, a performance better than those of leading nitrogen-doped carbon catalysts described in recent literatures (Table S2). Practically, the specific activity and costs are two crucial factors that dictate their applications. The reduced loading of catalysts not only facilitates mass transfer in the cathode, but also lowers the costs of cathode fabrication. Taken together, these results demonstrate that NCA800 indeed can serve as a low-cost catalyst for MFC air cathode, with a power output competitive to that of Pt/C.

Conclusion

In this study, NCAs were prepared by pyrolysis of polyacrylonitrile that served as a C and N source at controlled temperatures. The obtained carbon aerogels exhibited a high nitrogen dopant concentration up to 24 at.% and hence apparent ORR activity in alkaline media. The sample prepared at 800 °C outperformed others in the series, and was very competitive to commercial Pt/C. The remarkable performance was ascribed to the relatively high graphitic-N concentration (over 5 at.%) in the sample, along with a high degree of graphitization that dictated the electrical conductivity of the aerogels and accessibility of the electrocatalytic active centers. Using the as-prepared NCA as the catalyst for an MFC air cathode, the cell voltage and power density were

almost the same as those with Pt/C. These results indicate that NCAs can serve as viable, platinum-free, air cathode catalysts for MFC applications.

ASSOCIATED CONTENT

Supporting Information. Additional voltammetric data and fitting results of electrochemical impedance spectra. The files are available free of charge from the authors or from the webpage at http://pubs.acs.org.

AUTHOR INFORMATION

Corresponding Author

* E-mail: lijun@cqu.edu.cn (J.L.), shaowei@ucsc.edu (S.W.C.)

Author Contributions

The manuscript was written through contributions of all authors. All authors have given approval to the final version of the manuscript.

fellowship. TEM and XPS studies were performed at the National Center for Electron Microscopy and Molecular Foundry of the Lawrence Berkeley National Laboratory as part of a user project.

REFERENCES

1. Liao, Q.; Zhu, X.; Zheng, X. Y.; Ding, Y. D., Visualization study on the dynamics of CO2 bubbles in anode channels and performance of a DMFC. *J Power Sources* **2007,** *171*, 644-651.
2. Zhu, X.; Liao, Q.; Sui, P. C.; Djilali, N., Numerical investigation of water droplet dynamics in a low-temperature fuel cell microchannel: Effect of channel geometry. *J Power Sources* **2010,** *195*, 801-812.
3. Liu, X.; Guo, H.; Ye, F.; Ma, C. F., Water flooding and pressure drop characteristics in flow channels of proton exchange membrane fuel cells. *Electrochim Acta* **2007,** *52*, 3607-3614.
4. Liu, X.; Guo, H.; Ma, C. F., Water flooding and two-phase flow in cathode channels of proton exchange membrane fuel cells. *J Power Sources* **2006,** *156*, 267-280.
5. Santoro, C.; Serov, A.; Gokhale, R.; Rojas-Carbonell, S.; Stariha, L.; Gordon, J.; Artyushkova, K.; Atanassov, P., A family of Fe-NC oxygen reduction electrocatalysts for microbial fuel cell (MFC) application: relationships between surface chemistry and performances. *Appl Catal B: Environ* **2017,** *205*, 24-33.
6. Trapero, J. R.; Horcajada, L.; Linares, J. J.; Lobato, J., Is microbial fuel cell technology ready? An economic answer towards industrial commercialization. *Appl Energy* **2017,** *185*, 698-707.
7. You, S.; Gong, X.; Wang, W.; Qi, D.; Wang, X.; Chen, X.; Ren, N., Enhanced Cathodic Oxygen Reduction and Power Production of Microbial Fuel Cell Based on Noble‐Metal‐Free Electrocatalyst Derived from Metal‐Organic Frameworks. *Adv Energy Mater* **2016,** *6*, 1501497.
8. Chen, S. C.; Chen, Z. H.; Siahrostami, S.; Kim, T. R.; Nordlund, D.; Sokaras, D.; Nowak, S.; To, J. W. F.; Higgins, D.; Sinclair, R.; Norskov, J. K.; Jaramillo, T. F.; Bao, Z. A., Defective Carbon-Based Materials for the Electrochemical Synthesis of Hydrogen Peroxide. *Acs Sustain Chem Eng* **2018,** *6*, 311-317.
9. Barros, W. R. P.; Ereno, T.; Tavares, A. C.; Lanza, M. R. V., In Situ Electrochemical Generation of Hydrogen Peroxide in Alkaline Aqueous Solution by using an Unmodified Gas Diffusion Electrode. *Chemelectrochem* **2015,** *2*, 714-719.
10. Daems, N.; Sheng, X.; Vankelecom, I. F.; Pescarmona, P. P., Metal-free doped carbon materials as electrocatalysts for the oxygen reduction reaction. *J Mater Chem A* **2014,** *2*, 4085-4110.
11. Zhang, X.; He, W.; Zhang, R.; Wang, Q.; Liang, P.; Huang, X.; Logan, B. E.; Fellinger, T. P., High‐Performance Carbon Aerogel Air Cathodes for Microbial Fuel Cells. *Chemsuschem* **2016,** *9*, 2788-2795.
12. Feng, L.; Yan, Y.; Chen, Y.; Wang, L., Nitrogen-doped carbon nanotubes as efficient and durable metal-free cathodic catalysts for oxygen reduction in microbial fuel cells. *Energy Environ Sci* **2011,** *4*, 1892-1899.

13. Cheng, S.; Liu, H.; Logan, B. E., Increased performance of single-chamber microbial fuel cells using an improved cathode structure. *Electrochem Commun* **2006,** *8*, 489-494.
14. Quan, X.; Mei, Y.; Xu, H.; Sun, B.; Zhang, X., Optimization of Pt-Pd alloy catalyst and supporting materials for oxygen reduction in air-cathode Microbial Fuel Cells. *Electrochim Acta* **2015,** *165*, 72-77.
15. Yang, T.; Li, K.; Pu, L.; Liu, Z.; Ge, B.; Pan, Y.; Liu, Y., Hollow-spherical Co/NC nanoparticle as an efficient electrocatalyst used in air cathode microbial fuel cell. *Biosens Bioelectron* **2016,** *86*, 129-134.
16. Peng, Y.; Chen, S., Electrocatalysts Based on Metal@Carbon Core@Shell Nanocomposites: an Overview. *Green Energy Environ* **2018**, *3*, 335-351
17. Liu, Y.; Li, K.; Liu, Y.; Pu, L.; Chen, Z.; Deng, S., The high-performance and mechanism of P-doped activated carbon as a catalyst for air-cathode microbial fuel cells. *J Mater Chem A* **2015,** *3*, 21149-21158.
18. Peng, Y.; Lu, B.; Chen, S., Carbon-Supported Single Atom Catalysts for Electrochemical Energy Conversion and Storage. *Adv Mater* **2018**, *30*, 1801995.
19. Xia, X.; Zhang, F.; Zhang, X.; Liang, P.; Huang, X.; Logan, B. E., Use of pyrolyzed iron ethylenediaminetetraacetic acid modified activated carbon as air–cathode catalyst in microbial fuel cells. *ACS Appl Mater Interfaces* **2013,** *5*, 7862-7866.
20. Zhang, X.; Xia, X.; Ivanov, I.; Huang, X.; Logan, B. E., Enhanced activated carbon cathode performance for microbial fuel cell by blending carbon black. *Environ Sci Technol* **2014,** *48*, 2075-2081.
21. Yang, W.; Li, J.; Ye, D.; Zhu, X.; Liao, Q., Bamboo charcoal as a cost-effective catalyst for an air-cathode of microbial fuel cells. *Electrochim Acta* **2017,** *224*, 585-592.
22. Fan, Z.; Li, J.; Zhou, Y.; Fu, Q.; Yang, W.; Zhu, X.; Liao, Q., A green, cheap, high-performance carbonaceous catalyst derived from Chlorella pyrenoidosa for oxygen reduction reaction in microbial fuel cells. *Int J Hydrogen Energy* **2017,** *42*, 27657-27665.
23. Liang, J.; Jiao, Y.; Jaroniec, M.; Qiao, S. Z., Sulfur and Nitrogen Dual-Doped Mesoporous Graphene Electrocatalyst for Oxygen Reduction with Synergistically Enhanced Performance. *Angew Chem Int Edit* **2012,** *51*, 11496-11500.
24. Zhou, L.; Fu, P.; Cai, X.; Zhou, S.; Yuan, Y., Naturally derived carbon nanofibers as sustainable electrocatalysts for microbial energy harvesting: A new application of spider silk. *Appl Catal B: Environ* **2016,** *188*, 31-38.
25. Wang, Q.; Zhang, X.; Lv, R.; Chen, X.; Xue, B.; Liang, P.; Huang, X., Binder-free nitrogen-doped graphene catalyst air-cathodes for microbial fuel cells. *J Mater Chem A* **2016,** *4*, 12387-12391.
26. Zhou, L. H.; Fu, P.; Wen, D. H.; Yuan, Y.; Zhou, S. G., Self-constructed carbon nanoparticles-coated porous biocarbon from plant moss as advanced oxygen reduction catalysts. *Appl Catal B-Environ* **2016,** *181*, 635-643.
27. Yang, H.; Dong, J.; Hong, Y.; Lin, W.; Zhou, Z.; Sun, S., Comparative investigation of CO_2 and oxygen reduction on Fe/N/C catalysts. *Electrochem Commun* **2018,** *97*, 82-86.
28. Tian, X. Y.; Zhou, M. H.; Tan, C. L.; Li, M.; Liang, L.; Li, K. R.; Su, P., KOH activated N-doped novel carbon aerogel as efficient metal-free oxygen reduction catalyst for microbial fuel cells. *Chem Eng J* **2018,** *348*, 775-785.
29. Tardy, G. M.; Lorant, B.; Loka, M.; Nagy, B.; Laszlo, K., Enhancing substrate utilization and power production of a microbial fuel cell with nitrogen-doped carbon aerogel as cathode catalyst. *Biotechnol Lett* **2017,** *39*, 993-999.

30. Salvador, G. P.; Gerosa, M.; Sacco, A.; Garino, N.; Castellino, M.; Massaglia, G.; Delmondo, L.; Agostino, V.; Margaria, V.; Chiodoni, A.; Quaglio, M., Green-Synthesized Nitrogen-Doped Carbon-Based Aerogels as Environmentally Friendly Catalysts for Oxygen Reduction in Microbial Fuel Cells. *Energy Technol-Ger* **2018,** *6*, 1052-1059.

31. Watson, V. J.; Delgado, C. N.; Logan, B. E., Improvement of activated carbons as oxygen reduction catalysts in neutral solutions by ammonia gas treatment and their performance in microbial fuel cells. *J Power Sources* **2013,** *242*, 756-761.

32. You, C.; Liao, S.; Li, H.; Hou, S.; Peng, H.; Zeng, X.; Liu, F.; Zheng, R.; Fu, Z.; Li, Y., Uniform nitrogen and sulfur co-doped carbon nanospheres as catalysts for the oxygen reduction reaction. *Carbon* **2014,** *69*, 294-301.

33. Ge, Z.; He, Z., An effective dipping method for coating activated carbon catalyst on the cathode electrodes of microbial fuel cells. *RSC Adv* **2015,** *5*, 36933-36937.

34. Dong, H.; Yu, H.; Wang, X.; Zhou, Q.; Feng, J., A novel structure of scalable air-cathode without Nafion and Pt by rolling activated carbon and PTFE as catalyst layer in microbial fuel cells. *Water Res* **2012,** *46*, 5777-5787.

35. Fang, Y.; Gu, D.; Zou, Y.; Wu, Z.; Li, F.; Che, R.; Deng, Y.; Tu, B.; Zhao, D., A low-concentration hydrothermal synthesis of biocompatible ordered mesoporous carbon nanospheres with tunable and uniform size. *Angew Chem Int Edit* **2010,** *122*, 8159-8163.

36. Wei, W.; Liang, H. W.; Parvez, K.; Zhuang, X. D.; Feng, X. L.; Mullen, K., Nitrogen-Doped Carbon Nanosheets with Size-Defined Mesopores as Highly Efficient Metal-Free Catalyst for the Oxygen Reduction Reaction. *Angew Chem Int Edit* **2014,** *53*, 1570-1574.

37. Wang, Q. F.; Zou, R. Q.; Xia, W.; Ma, J.; Qiu, B.; Mahmood, A.; Zhao, R.; Yang, Y. Y. C.; Xia, D. G.; Xu, Q., Facile Synthesis of Ultrasmall CoS2 Nanoparticles within Thin N-Doped Porous Carbon Shell for High Performance Lithium-Ion Batteries. *Small* **2015,** *11*, 2511-2517.

38. Wohlgemuth, S.-A.; White, R. J.; Willinger, M.-G.; Titirici, M.-M.; Antonietti, M., A one-pot hydrothermal synthesis of sulfur and nitrogen doped carbon aerogels with enhanced electrocatalytic activity in the oxygen reduction reaction. *Green Chem* **2012,** *14*, 1515-1523.

39. Wang, J.; Wu, H.; Gao, D.; Miao, S.; Wang, G.; Bao, X., High-density iron nanoparticles encapsulated within nitrogen-doped carbon nanoshell as efficient oxygen electrocatalyst for zinc–air battery. *Nano Energy* **2015,** *13*, 387-396.

40. Liu, X. J.; Li, L. G.; Zhou, W. J.; Zhou, Y. C.; Niu, W. H.; Chen, S. W., High-Performance Electrocatalysts for Oxygen Reduction Based on Nitrogen-Doped Porous Carbon from Hydrothermal Treatment of Glucose and Dicyandiamide. *Chemelectrochem* **2015,** *2*, 803-810.

41. Niu, W. H.; Li, L. G.; Liu, X. J.; Wang, N.; Liu, J.; Zhou, W. J.; Tang, Z. H.; Chen, S. W., Mesoporous N-Doped Carbons Prepared with Thermally Removable Nanoparticle Templates: An Efficient Electrocatalyst for Oxygen Reduction Reaction. *J Am Chem Soc* **2015,** *137*, 5555-5562.

42. Liu, X. J.; Zou, S. Z.; Chen, S. W., Ordered mesoporous carbons codoped with nitrogen and iron as effective catalysts for oxygen reduction reaction. *Nanoscale* **2016,** *8*, 19249-19255.

43. Lu, B. Z.; Smart, T. J.; Qin, D. D.; Lu, J. E.; Wang, N.; Chen, L. M.; Peng, Y.; Ping, Y.; Chen, S. W., Nitrogen and Iron-Codoped Carbon Hollow Nanotubules as High-Performance Catalysts toward Oxygen Reduction Reaction: A Combined Experimental and Theoretical Study. *Chem Mater* **2017,** *29*, 5617-5628.

44. Wang, N.; Lu, B. Z.; Li, L. G.; Niu, W. H.; Tang, Z. H.; Kang, X. W.; Chen, S. W., Graphitic

Nitrogen Is Responsible for Oxygen Electroreduction on Nitrogen-Doped Carbons in Alkaline Electrolytes: Insights from Activity Attenuation Studies and Theoretical Calculations. *Acs Catal* **2018,** *8*, 6827-6836.

45. Lai, L.; Potts, J. R.; Zhan, D.; Wang, L.; Poh, C. K.; Tang, C.; Gong, H.; Shen, Z.; Lin, J.; Ruoff, R. S., Exploration of the active center structure of nitrogen-doped graphene-based catalysts for oxygen reduction reaction. *Energy Environ Sci* **2012,** *5*, 7936-7942.

Table 1. Summary of structural characteristics and ORR activities of the NCA series

Sample	NC600	NC700	NC800	NC900
C (at.%)	58.72	59.47	73.48	71.51
N (at.%)	23.39	8.51	13.56	10.41
O (at.%)	17.88	32.02	12.96	18.09
Pyridinic-N (at.%)	6.15	2.61	4.28	3.30
Pyrrolic-N (at.%)	12.15	3.78	4.08	2.48
Graphitic-N (at.%)	5.09	2.11	5.20	4.61
I_D/I_G	2.31	2.21	1.56	1.37
$E_{1/2}$ (V)	0.72	0.75	0.8	0.79
E_{onset} (V)	0.81	0.82	0.85	0.85
Tafel slope (mV dec^{-1})	91.3	49	30.1	38.8
j_K (mA cm^{-2})	7.41	12.05	20.25	11.36
C_{dl} (mF cm^{-2})	5.69×10^{-2}	8.78×10^{-1}	1.41	5.52×10^{-1}

Graphical abstract
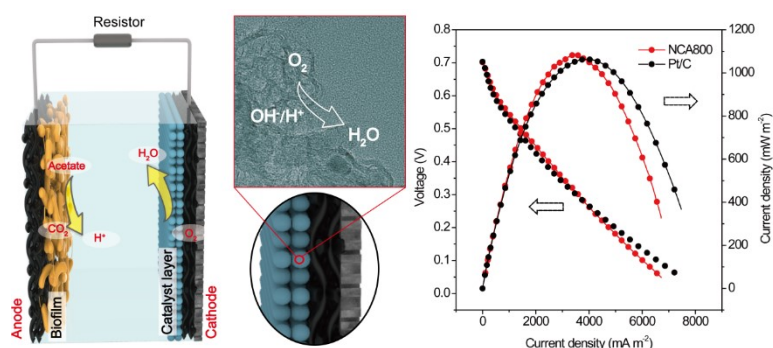
MFC is a unique technology for sustainable production of electricity and concurrently wastewater treatment. N-doped carbon aerogels can serve as effective air cathode catalysts.